

Coupling of GHz Phonons to Ferroelastic Domain Walls in SrTiO₃

L. Maerten,¹ A. Bojahr,¹ M. Gohlke,¹ M. Rössle,¹ and M. Bargheer^{1,2,*}

¹Institut für Physik & Astronomie, Universität Potsdam, Karl-Liebknecht-Strasse 24-25, 14476 Potsdam, Germany

²Helmholtz-Zentrum-Berlin für Energie und Materialforschung, Wilhelm-Conrad-Röntgen Campus,
BESSY II, Albert-Einstein-Strasse 15, 12489 Berlin, Germany

(Received 1 November 2013; published 28 January 2015)

We study the linear and nonlinear acoustic response of SrTiO₃ across its ferroelastic transition at $T_a = 105$ K by time domain Brillouin scattering. Above T_a we observe that for a strain amplitude of $\sim 0.18\%$ the sound velocity for compressive strain exceeds the tensile strain velocity by 3%. Below T_a we find a giant slowing down of the sound velocity by 12% and attribute this to the coupling of GHz phonons to ferroelastic twin domain walls. We propose a new mechanism for this coupling on the ultrafast time scale, providing an important new test ground for theories used to simulate atomic motion in domain forming crystals.

DOI: 10.1103/PhysRevLett.114.047401

PACS numbers: 78.35.+c, 62.25.Fg, 63.20.Ry, 78.20.hc

SrTiO₃ (STO) is a dielectric perovskite which exhibits quantum paraelectric behavior at low temperatures [1]. It is widely used as a substrate material for the growth of perovskite thin films, e.g., to create novel nanoelectronic phenomena and applications. Hence, understanding the dynamics of the domain pattern in the substrate is crucial [2,3]. The various structural phase transitions and the domain pattern of STO have been subject to extensive research [4–12]. The elastic behavior of STO has been studied since the 1960s [13–16] and has recently attracted attention due to the observation of a very high mobility of domain walls in the antiferrodistortive phase [5,17].

STO undergoes an antiferrodistortive phase transition at $T_a = 105$ K, where the oxygen octahedra in adjacent unit cells rotate against each other around one of the cubic axes [18]. This motion is described by a triply degenerate optical zone edge mode, which softens towards the phase transition [11,19]. It is accompanied by a doubling of the unit cell and a small tetragonal elongation of the c axis oriented parallel to the rotational axis of the octahedra [4,11]. Domains are formed with the elongated axis oriented in one of the three possible directions. The formation of these so-called twin domains can be suppressed by external pressure [17,20], is altered near the crystal surface [12], and is strongly influenced by the presence of a surface layer [10]. The coupling of acoustic phonons to the soft optic mode leads to an anomaly in the acoustic properties [13,21] of the material and to an increased dissipation at the phase transition [15,16,22]. The induced softening of the acoustic modes at the transition is superimposed by an even larger softening below T_a that can be attributed to the coupling of phonons to domain walls between areas of differently oriented c axes (twin walls) and has been termed superelastic behavior [17]. This additional softening is minimized, when the domain formation is reduced, for example by external pressure [17,20]. The data compilation by

Carpenter shows a large variation of the sound velocity below T_a [9]. However, all data obtained by Brillouin scattering, i.e., experiments sensitive to GHz phonons, show only the small drop in sound velocity at T_a that is attributed to the coupling to the soft mode [22–24].

In this Letter we study the elastic behavior of STO by time domain Brillouin scattering (TDBS) [25]. We start in the regime of linear response and extend our measurements into the regime of nonlinear sound propagation. The amplitude of the strain pulses is calibrated using ultrafast x-ray diffraction (UXRD) [26,27]. When the hypersound strain amplitude exceeds $\sim 0.1\%$, we observe a giant reduction of the sound velocity below T_a , similar to the superelastic behavior observed for low frequency strain. This was previously thought to be impossible for GHz frequencies [17,28,29]. Our experiments suggest that this phenomenon occurs for GHz sound only when the strain amplitude is large enough to establish a new mechanism for coupling to the twin walls. It is enabled when the transient unit cell deformation exceeds the tetragonal distortion. We argue that under these conditions the velocity of the domain wall motion approaches the sound velocity and that the relevant time scale enabling full superelastic behavior is determined by the time $\tau = D/v_s$ it takes lattice deformations to propagate through the average size D of the domains at the speed of sound v_s .

We use optical pump pulses with a wavelength of 800 nm and 120 fs pulse duration at a repetition rate of 5 kHz to excite few nanometer thick metal transducer films on STO substrates. We use excitation fluences in the range between 15 and 45 mJ/cm². The rapid expansion of the metal film launches bipolar strain pulses into the STO which are probed by TDBS: an ultrashort white light continuum pulse generated in a sapphire disc is reflected from the sample and spectrally resolved by a fiber-optic spectrometer for broadband detection [25,26]. This method

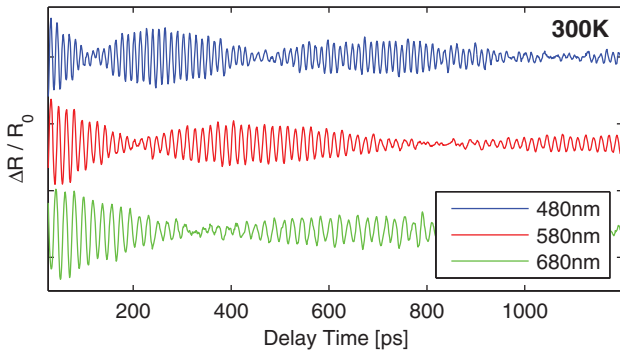


FIG. 1 (color). Transient reflectivity change at room temperature for high excitation fluences, plotted for different probe wavelengths. The curves are shifted vertically for clarity.

relies on the interference of the probe light reflected from the sample surface with a component reflected from the traveling strain pulse. Constructive interference is given when the optical path difference between the interfering light beams amounts to integer multiples of the light wavelength. This leads to a transient reflectivity signal which oscillates at the frequency

$$\nu(\lambda) = v_s 2n(\lambda) \cos(\beta)/\lambda, \quad (1)$$

where λ is the probe wavelength, β is the internal angle of incidence with respect to the surface normal, and $n(\lambda)$ the wavelength dependent refractive index extracted from the literature [30]. The measured oscillation frequency $\nu(\lambda)$ is equal to the frequency $\nu_{ph}(k_{ph})$ of the observed phonon with wave vector $k_{ph} = 2\pi/\lambda_{ph} = 2\pi n(\lambda) \cos(\beta)/\lambda$, for which the Brillouin backscattering condition is fulfilled [25]. Here, λ_{ph} is the wavelength of the detected phonon. The sample is mounted in a closed cycle refrigerator allowing for a temperature dependent series of measurements.

We mainly discuss experimental data obtained from a 37 nm thick $(La_{0.7}Sr_{0.3})MnO_3$ (LSMO) transducer grown by pulsed laser deposition onto a single-crystalline (100)-STO substrate (CrysTec, Berlin, miscut angle of 0.1°) [31]. Several similar samples have been measured in order to verify the conclusions, as will be discussed in the text below. Figure 1 shows high fluence data for three selected probe wavelengths at room temperature. The raw data are cut shortly after the fast electronic response at $t = 0$ and a slowly varying background is subtracted. The remaining signal oscillates at the frequency given by Eq. (1). In addition, the signal oscillations are modulated by a slow beating

$$\nu_{beating} = \Delta v_s 2n(\lambda) \cos(\beta)/\lambda, \quad (2)$$

which can be attributed to the difference Δv_s of the sound velocities present in the material [26]. In this case, for large

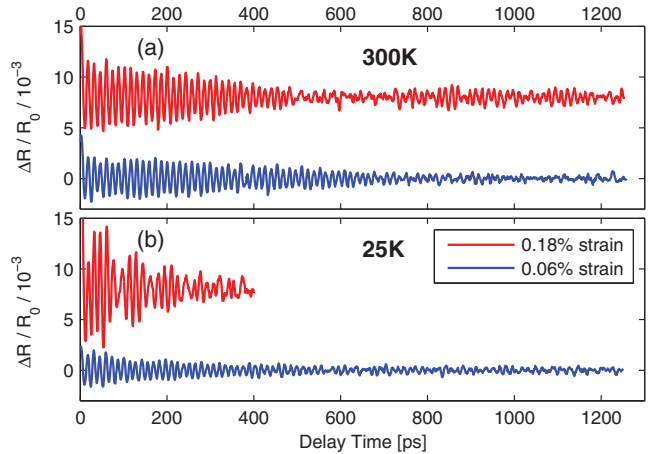


FIG. 2 (color). Transient reflectivity traces for (a) $T = 300$ K and (b) $T = 25$ K and two different strain amplitudes evaluated at $\lambda = 528$ nm ($\nu = 71$ GHz). The curves are shifted vertically for clarity.

amplitude strain in STO at room temperature, the sound velocity for compressive strain is larger than that for tensile strain. This is supported by calculations using an anharmonic linear chain model [26] and by UXRD experiments using acoustic pulse trains [32]. In Fig. 2 the beating is only present for large strain amplitudes (red curves). In the linear regime (low fluence, blue curves), we obtain a single Brillouin oscillation frequency $\nu(\lambda)$, i.e., a single value for the sound velocity. The amplitude of the generated sound pulse in STO has been calibrated by measuring the maximum expansion of the LSMO film after 6 ps using UXRD with 200 fs time resolution [26]. The strain amplitude in the STO amounts to half of the maximum strain in the LSMO weighted by the ratio of the sound velocities [13,26,33]. Figure 2(a) shows two measurements at room temperature. Figure 2(b) shows the same traces for $T = 25$ K, which look similar to the room temperature data for small strain amplitudes. The beating frequency for high excitation, however, is strongly temperature dependent. Additionally, we note that in the high excitation regime the oscillations are damped out comparatively fast. The Fourier transform of the signal yields the oscillation frequencies from which the sound velocity can be computed according to Eq. (1). The result is a velocity distribution [26], which reflects the fact that for large amplitude waves, compressive and tensile strains propagate at different sound velocities [32,34]. We extract the sound velocities for all temperatures at small and large strain levels. Figure 3(a) shows the sound velocity distribution for high excitation at four different temperatures computed from the signal at $\lambda = 528$ nm ($\nu \approx 70$ GHz). Figure 3(b) collects the maxima of the sound velocity distributions for low (open circles) and high (full circles) excitation as a function of temperature. In the linear regime, a sudden softening at the phase transition is observed in quantitative agreement with the literature

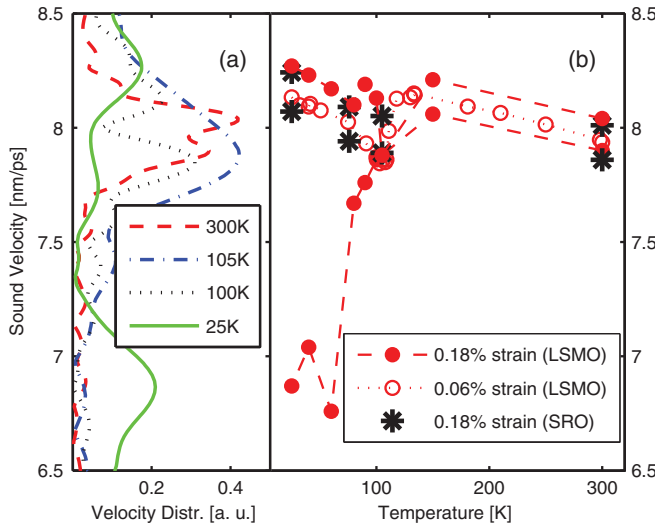


FIG. 3 (color). (a) Sound velocity distribution extracted from the Fourier transform of the transient reflectivity data shown in Fig. 2, for 0.18% strain amplitude in STO at selected temperatures generated by excitation of an LSMO transducer. (b) Extracted maxima from panel (a) as a function of temperature. Red open and full circles: sound velocities in STO for the LSMO transducer; black stars: sound velocities in STO for the SRO transducer. For strain amplitude refer to legend.

[14,22]. This softening close to the phase transition originates from the coupling of the strain wave to the soft mode describing the structural phase transition at T_a [9]. In the nonlinear regime and at temperatures above T_a we observe a temperature independent, symmetric splitting, which can be explained by the anharmonicity of the interatomic potential, as discussed in detail for the room temperature data [26]. Below T_a a giant reduction of the sound velocity is observed that exceeds the symmetric splitting and cannot only be explained by anharmonicity [35–37]. This reduction is comparable to the superelastic softening of the elastic constants in STO which has so far only been found for lower frequency phonons in the Hz to MHz regime and is attributed to the coupling of phonons to (twin) domain walls [5,17,20,28,29]. It is accompanied by an increased damping, which is observed for the low T high fluence data in Fig. 2. The scattering of the data at low T in Fig. 3 might be due to additional phase transitions discussed in the literature [4,5,17].

We confirm that the giant softening for large amplitude GHz strain waves originates from the coupling to twin walls by repeating the experiments for similar samples with different epitaxial strain conditions: we used two STO samples with 15 nm and 70 nm thick SrRuO₃ (SRO) transducer films and 20, 37, and 90 nm thick LSMO films. SRO transducers lead to a tensile strain at the interface, and therefore to a compressive out-of-plane strain in the STO substrate material. This suppresses the formation of domains with the elongated tetragonal c axis parallel to the direction of the strain pulse traveling perpendicular to

the surface in a similar way [38] as observed for static external stress [17,20,39].

In contrast, x-ray diffraction measurements on STO with a thin YBa₂Cu₃O₇ top layer prove that a transducer with a smaller lattice constant, such as LSMO, leads to mixed domains with the c axis aligned either parallel or perpendicular to the surface within the first micrometers of the STO substrate [10]. Indeed, all samples with LSMO transducers show a giant softening due to the interactions with the twin walls, while samples with SRO transducers should not. Low fluence TDBS data for the samples with SRO transducers (not shown) yield sound velocities in agreement with LSMO transducers for small strain levels [open symbols in Fig. 3(a)]. For large strain amplitudes the data obtained from SRO transducers (black stars in Fig. 3) are in accord with the results for LSMO transducers only for temperatures above T_a . Below T_a the sound velocity exhibits the same small but symmetric splitting of the sound velocities observed above T_a . These experiments with SRO transducers show that the alignment of the long c axis relative to the sample surface also removes the coupling of large amplitude GHz strain to the domain walls. The measurements with LSMO samples of different thicknesses (20 and 90 nm) confirm the results for the 37 nm LSMO film reported above.

Figure 4(a) visualizes a twin wall in STO according to the literature [2,3]. The shaded grey area visualizes the stress in the crystal in the vicinity of a kink in the wall as observed in simulations [7,8]. In the following we call the region on the upper left side of the domain wall A where the long c axis is perpendicular to \mathbf{k}_{ph} . The region on the lower right with the c axis oriented along \mathbf{k}_{ph} is addressed as B. For a slow and small expansion of the crystal, the domain wall travels by moving the kink parallel to the wall along the thin black arrow [7,17]. This increases domains with the c axis along \mathbf{k}_{ph} and decreases region A. In total, the crystal is expanded more along \mathbf{k}_{ph} than without domain wall motion. The crystal appears to be softer; i.e., it has a reduced sound velocity. This process requires a contraction of the crystal perpendicular to the applied stress by the Poisson effect and additionally due to the decreasing number of unit cells with the long c axis perpendicular to the stress. For a homogeneous expansion over the diameter $d_L = 100 \mu\text{m}$, given by the laser excited area, the in-plane contraction would take place on a time scale exceeding $\tau \sim d_L/v_s \sim 12 \text{ ns}$, determined by the time it takes to relax the strain at the sound velocity v_s . This restricts the superelastic regime to the 80 MHz range on a 100 μm length scale. For GHz phonons or picosecond strain pulses in the linear regime, twin wall motion is fully suppressed [28,29].

In the nonlinear regime we propose the following mechanism: The transducer with thickness d generates strain waves with wave vector \mathbf{k}_{ph} perpendicular to the sample surface. The fundamental wavelength

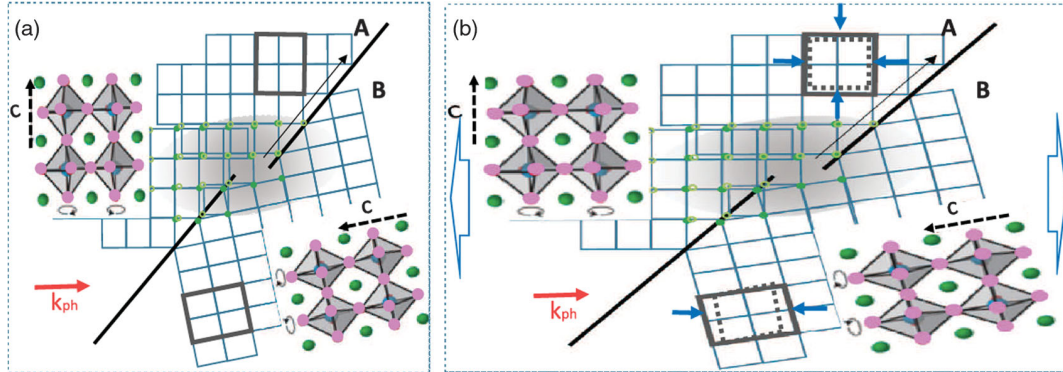


FIG. 4 (color). (a) Schematic of the STO crystal in the tetragonal phase near a kink in a twin wall according to literature [2,3,7,8]. Tetragonal distortion and twinning angle are exaggerated. The shaded grey region highlights the strain field near the kink. (a) Black line: twin wall with kink. Grey rectangles: unit cells of tetragonal phase. Details of these unit cells are shown with oxygen octahedra as enlarged insets. For slow vertical expansion the kink would move along the thin black arrow. (b) Snapshot for ultrafast uniaxial expansive strain along \mathbf{k}_{ph} with amplitude exceeding the original tetragonal distortion (see text). No contraction perpendicular to \mathbf{k}_{ph} can occur for this time scale. Blue narrow arrows: compressive forces that counteract the external uniaxial expansion.

$\lambda_{ph} = 2\pi/k_{ph} \leq 2d$ of the strain wave is limited by the thickness d or the optical penetration depth ξ of the exciting light in the transducer. The strain fronts are plane waves since the spot size of the exciting laser light $d_L = 100 \mu\text{m} \gg d$. We first discuss the effect on twin wall motion induced by the expansive part of the bipolar strain pulse. Strain with an amplitude (here 0.18%) much larger than the tetragonal distortion [4,18] ($(c-a)/a = 5 \times 10^{-4}$) leads to expanded tetragonal unit cells [40] in region A with the longer unit cell axis now parallel to \mathbf{k}_{ph} , as schematically shown by the solid grey rectangle in Fig. 4(b). These expanded unit cells in A want to contract in all three dimensions in order to recover their original volume (dotted grey rectangle). Within the domains, all stresses are balanced by adjacent unit cells. In region B the unit cells feel compressive stress (blue arrows) only along \mathbf{k}_{ph} . Thus, at the domain wall the stress perpendicular to \mathbf{k}_{ph} is unbalanced and leads to a motion of the domain wall and the connected strain fields such that region B increases. The reverse effect would be expected for the compressive part of the strain pulse. However, since space is required for the atoms at the domain boundary to rearrange, the coupling is mainly observed for tensile strain.

Figure 4(b) suggests complex microscopic dynamics. The moving domain walls do not separate domains in their equilibrium structure, but rather domains of the crystal with tetragonal nonequilibrium strain. The increased damping and the superelastic effect are intimately connected to propagation of nonequilibrium strain fields around kinks in the twin walls. The importance of lattice inhomogeneities for the propagation of strain waves is emphasized in related experiments: in ferroelectric $\text{Pb}(\text{Zr}_{0.2}\text{Ti}_{0.8})\text{O}_3$ we have observed by UXRD that the sign, amplitude, and frequency of the strain pulses alter the interaction with domain boundaries and dislocations [41]. Similar dependences on the frequency and amplitude of the applied strains

are reported for the velocity of ferroelastic [42] and ferroelectric [43] domain wall motion.

The considerable additional softening at 70 GHz indicates that the twin walls propagate a substantial fraction of the domain size [6] $D \sim 100 \text{ nm}$ within a half period τ of the sound wave. Therefore, the domain wall velocity must be on the order of the sound velocity. Computer simulations on the terahertz time scale have indicated kink-propagation velocities exceeding the sound velocity [8]. Our 12% reduction in sound velocity for 70 GHz large amplitude strain compares to a 50% reduction of the Young's modulus measured at 10 Hz [17]; i.e., we observe about half the softening effect.

In summary, we have performed time domain Brillouin-scattering experiments and measured the sound velocity in STO at different temperatures for various strain amplitudes. In the nonlinear regime of $\sim 0.18\%$ strain the sound velocity of compressive strain exceeds the velocity for tensile strain by 3% for temperatures above $T_a = 105 \text{ K}$. Below T_a a substantial softening of 12% is observed, which is attributed to a coupling of the GHz longitudinal phonons to twin domain walls. This behavior is observed for transient strains exceeding the tetragonal distortion in the low temperature phase, suggesting a different mechanism inducing the domain wall motion than for lower, Hz to MHz frequency sound. Our observations highlight the importance of understanding the coupling of strain waves to domain walls in domain forming samples. Our UXRD calibrated measurements provide a good testing ground for simulations attempting to predict the domain dynamics accompanying structural phase transitions in complex oxides.

We thank I. Vrejoiu and D. Schlom for providing the samples. We acknowledge the financial support by the Leibniz Graduate school DinL and the BMBF via 05K2012–OXIDE.

- *bargheer@uni-potsdam.de; www.udkm.physik.uni-potsdam.de.
- [1] K. A. Müller and H. Burkard, *Phys. Rev. B* **19**, 3593 (1979).
- [2] M. Honig, J. A. Sulpizio, J. Drori, A. Joshua, E. Zeldov, S. Ilani, and W. Schranz, *Nat. Mater.* **12**, 1112 (2013).
- [3] B. Kalisky *et al.*, *Nat. Mater.* **12**, 1091 (2013).
- [4] F. W. Lytle, *J. Appl. Phys.* **35**, 2212 (1964).
- [5] J. F. Scott, E. K. H. Salje, and M. A. Carpenter, *Phys. Rev. Lett.* **109**, 187601 (2012).
- [6] J. Chrosch and E. K. H. Salje, *J. Phys. Condens. Matter* **10**, 2817 (1998).
- [7] E. K. H. Salje, X. Ding, Z. Zhao, T. Lookman, and A. Saxena, *Phys. Rev. B* **83**, 104109 (2011).
- [8] E. Salje, Z. Zhao, X. Ding, and J. Sun, *Am. Mineral.* **98**, 1449 (2013).
- [9] M. A. Carpenter, *Am. Mineral.* **92**, 309 (2007).
- [10] R. Loetsch, A. Lübcke, I. Uschmann, E. Foerster, V. Grosse, M. Thuerk, T. Koettig, F. Schmidl, and P. Seidel, *Appl. Phys. Lett.* **96**, 071901 (2010).
- [11] G. Shirane and Y. Yamada, *Phys. Rev.* **177**, 858 (1969).
- [12] Z. Salman, M. Smadella, W. A. MacFarlane, B. D. Patterson, P. R. Willmott, K. H. Chow, M. D. Hossain, H. Saadaoui, D. Wang, and R. F. Kiefl, *Phys. Rev. B* **83**, 224112 (2011).
- [13] R. O. Bell and G. Rupprecht, *Phys. Rev.* **129**, 90 (1963).
- [14] W. Kaiser and R. Zurek, *Phys. Lett.* **23**, 668 (1966).
- [15] R. Nava, R. Callarotti, H. Ceva, and A. Martinet, *Phys. Rev.* **188**, 1456 (1969).
- [16] B. Berre, K. Fossheim, and K. A. Müller, *Phys. Rev. Lett.* **23**, 589 (1969).
- [17] A. V. Kityk, W. Schranz, P. Sondergeld, D. Havlik, E. K. H. Salje, and J. F. Scott, *Phys. Rev. B* **61**, 946 (2000).
- [18] H. Unoki and T. Sakudo, *J. Phys. Soc. Jpn.* **23**, 546 (1967).
- [19] T. Kohmoto, K. Tada, T. Moriyasu, and Y. Fukuda, *Phys. Rev. B* **74**, 064303 (2006).
- [20] K. Fossheim and B. Berre, *Phys. Rev. B* **5**, 3292 (1972).
- [21] P. A. Fleury, *J. Acoust. Soc. Am.* **49**, 1041 (1971).
- [22] A. Nagakubo, A. Yamamoto, K. Tanigaki, H. Ogi, N. Nakamura, and M. Hirao, *Jpn. J. Appl. Phys.* **51**, 07GA09 (2012).
- [23] M. Yamaguchi, T. Yagi, Y. Tsujimi, H. Hasebe, R. Wang, and M. Itoh, *Phys. Rev. B* **65**, 172102 (2002).
- [24] B. Hehlen, Z. Kallassy, and E. Courtens, *Ferroelectrics* **183**, 265 (1996).
- [25] A. Bojahr, M. Herzog, S. Mitzscherling, L. Maerten, D. Schick, J. Goldshteyn, W. Leitenberger, R. Shayduk, P. Gaal, and M. Bargheer, *Opt. Express* **21**, 21188 (2013).
- [26] A. Bojahr, M. Herzog, D. Schick, I. Vrejoiu, and M. Bargheer, *Phys. Rev. B* **86**, 144306 (2012).
- [27] D. Schick, A. Bojahr, M. Herzog, C. von Korff Schmising, R. Shayduk, W. Leitenberger, P. Gaal, and M. Bargheer, *Rev. Sci. Instrum.* **83**, 025104 (2012).
- [28] W. Schranz, *Phys. Rev. B* **83**, 094120 (2011).
- [29] W. Schranz, H. Kabelka, and A. Tröster, *Ferroelectrics* **426**, 242 (2012).
- [30] M. Cardona, *Phys. Rev.* **140**, A651 (1965).
- [31] I. Vrejoiu, M. Ziese, A. Setzer, P. D. Esquinazi, B. I. Birajdar, A. Lotnyk, M. Alexe, and D. Hesse, *Appl. Phys. Lett.* **92**, 152506 (2008).
- [32] R. Shayduk *et al.*, *Phys. Rev. B* **87**, 184301 (2013).
- [33] Y. H. Ren, M. Trigo, R. Merlin, V. Adyam, and Q. Li, *Appl. Phys. Lett.* **90**, 251918 (2007).
- [34] O. L. Muskens and J. I. Dijkhuis, *Phys. Rev. Lett.* **89**, 285504 (2002).
- [35] A. Hachemi, H. Hachemi, A. Ferhat-Hamida, and L. Louail, *Phys. Scr.* **82**, 025602 (2010).
- [36] K. S. Viswanathan and B. Subramanyam, *Pramana J. Phys.* **42**, 175 (1994).
- [37] See Supplemental Material at <http://link.aps.org/supplemental/10.1103/PhysRevLett.114.047401> for fluence dependent measurements and further discussion.
- [38] The lattice mismatch between SRO and STO amounts to 6×10^{-3} . A uniaxial pressure of 1 MPa, which reduces the superelastic effect by several tens of percent [17], corresponds at room temperature [13] to an induced strain of 3×10^{-6} and is hence orders of magnitude larger than the lattice mismatch in our experiment.
- [39] T. S. Chang, J. F. Holzrichter, G. F. Imbusch, and A. L. Schawlow, *Appl. Phys. Lett.* **17**, 254 (1970).
- [40] The memory of the original *c*-axis orientation is rapidly lost since the thermal oxygen octahedra-tilt motion is fast compared to the duration of the passing strain pulse [19].
- [41] D. Schick, A. Bojahr, M. Herzog, P. Gaal, I. Vrejoiu, and M. Bargheer, *Phys. Rev. Lett.* **110**, 095502 (2013).
- [42] R. J. Harrison, S. A. T. Redfern, and E. K. H. Salje, *Phys. Rev. B* **69**, 144101 (2004).
- [43] S. Lisenkov, I. Ponomareva, and L. Bellaiche, *Phys. Rev. B* **79**, 024101 (2009).